Improving Battery Thermal Management Using Design for Six Sigma Process

Andreas Vlahinos, Advanced Engineering Solutions; Castle Rock, CO, USA, Tel: 303 814-0455

Ken Kelly, John Rugh, Ahmad Pesaran[1]
National Renewable Energy Laboratory; 1617 Cole Blvd, Golden, CO 80401, USA, Tel: (303) 275-3000

[1] Corresponding Author
Ahmad Pesaran, Principal Engineer, ahmad_pesaran@nrel.gov, Tel: 303 275-4441, Fax: 303 275-4415

For presentation at the
20th Electric Vehicle Symposium, Long Beach, CA (November 15-18, 2003)

Abstract

Battery thermal control is an important factor for achieving desired performance and calendar life for multi-cell batteries in hybrid electric vehicles. Automakers and their battery suppliers are paying increased attention to battery thermal management, especially with regard to life and related warranty costs. A robust design for thermal management is needed to ensure that certain parameters remain within design specifications under a variety of ambient and load conditions. For example, cells/modules in a pack must remain below a maximum temperature, temperature differences between cells must be below a desired value, and parasitic power must not exceed a designed value. Finite element thermal analysis, along with optimization and design for six sigma processes were used to evaluate alternatives that reduce temperature distribution and improve overall temperature uniformity among cells. A transient thermal analysis was also performed using the FreedomCAR 40kW power-assist profile and the thermal response for various flow rates was presented. These methods showed how variation in input parameters and conflicting design constraints could be accounted for when designing battery thermal management systems. For this paper, we modeled a Panasonic prismatic NiMH module with air-cooling, but the techniques can be applied to any battery configuration.

Keywords: Batteries, hybrid electric vehicles, thermal analysis, thermal management, six-sigma.

1. Introduction

Battery temperature affects battery performance and life. Therefore, battery thermal management is a critical element for achieving desired performance and calendar life for battery packs in hybrid electric vehicles. Automakers and their suppliers are paying increased attention to battery thermal management to ensure that warranty costs for battery replacement are not exceeding projections. The battery in a hybrid electric vehicle (HEV) experiences a demanding thermal environment and must be heated during cold-weather operation and cooled during extended use and during warm-weather operation. A uniform temperature should be maintained among the battery's cells since cell-to-cell temperature variability leads to imbalances and reduced performance and also potentially reduces calendar life.

The thermal design process should consider the cell-to-cell variability in a multi-cell pack, which could lead to different battery electrical and thermal behavior. There is also variability in the mechanical design and method for heating or cooling each cell. In addition, the thermal design process should consider the impact of various design parameters such as state of charge, internal resistance, current amplitude, heat generation rate, fluid flow rate, cooling/heating fluid temperature, and various geometrical variations. The

goals of a battery thermal management system are to keep the battery below a certain temperature and minimize the temperature distribution in the pack, while using a minimum amount of energy.

The National Renewable Energy Laboratory (NREL) has analyzed and evaluated the thermal performance of state-of-the-art commercial batteries and helped industry to develop better thermal designs. Along with our experimental capabilities, we use finite element thermal analysis and optimization and design for six sigma processes to evaluate alternatives that reduce temperature distribution and improve overall temperature uniformity. For this paper, we modeled a Panasonic prismatic NiMH module (Figure 1) with air-cooling and applied the basic six sigma quality principles; but the techniques can be applied to any battery configuration with other cooling methods.

2. The Parametric Deterministic Model

NREL's tests of the Toyota Prius NiMH battery in and out of vehicle [1-2] have given us a good understanding of battery thermal characteristics and response to various power demands required by the vehicle. As the electrical power is discharged/charged from/to the battery during a drive cycle, the battery heats up, mostly due to ohmic inefficiencies. The Prius pack uses forced air between the modules for heat removal/exchange. A parametric finite element model that can predict the maximum temperature (Tmax) and the maximum differential temperature within the pack (dT) was built. The gap spacing (tgap) between the battery cells, the cooling fan flow rate (Frate), and the internal electric resistance (R) of the cells were considered to be the three input design variables. The core, plastic case, and air space were considered in the Finite Element Analysis (FEA) model. Figure 2 shows a cutout view of the solid model with the case in purple, the core in cyan, and dead air space in red. Table 1 lists the material properties used in the FEA model. Figure 3 shows a typical temperature distribution of the parametric deterministic FEA model.

Table 1: Physical Parameters of the Parametric Finite Element Model

	Battery Core Properties	**Module Plastic Coating**	**Air Properties**
Thermal conductivity (W/m K)	15.0	0.170	0.0258
Density (kg/m3)	2327	1930	1.10
Heat capacity (J/kg K)	810	910	1013
Internal resistance (ohms)	0.02	n/a	n/a
Battery current (amps)	15.0	n/a	n/a
Air gap between modules (m)	0.002	n/a	n/a

3. The Probabilistic Design Loop

We assumed that all three design variables would exhibit normal distribution with given mean (μ_{tgap}, μ_R, μ_{Frate}) and standard deviation (σ_{tgap}, σ_R, and σ_{Frate}) values (Figure 4). To perform the analysis, we made the following assumptions to capture various possibilities. The mean values of the air gap and flow rate were considered control variables.

1. The mean value of the internal resistance and standard deviations of all three input design variables were considered as noise variables since they were out of the control of the battery pack designer.
2. The mean value of the gap (μ_{tgap}) was allowed to vary within a range of 1 mm and 3 mm. The standard deviation of the gap was assumed to be 5% of the mean value $\sigma_{tgap} = 0.05*\mu_{tgap}$.
3. The mean value of the electric resistance of cells was allowed to vary within a range of 0.01 - 0.03 ohms. The standard deviation of resistance was assumed to be 10% of the mean value, $\sigma_R = 0.10*\mu_R$.

4. The mean value of the flow rate was allowed to vary within a range of 0.25 to 1.5 scfm per module. The standard deviation of the flow rate was assumed to be 15% of the mean value, $\sigma_{Frate} = 0.15*\mu_{Frate}$.

Given a set of mean values for these input design variables and an assumed distribution, one may easily generate a large set of random numbers for each variable. Several sampling techniques are available to generate combination sets of design variables including Monte Carlo, Latin Hypercube Sampling (LHS), Central Composite, Box-Behnken Matrix, etc. [3-7]. If the "experiment" is fast, the inexpensive Monte Carlo and LHS sampling techniques work well. If the "experiment" is time consuming and expensive, the Box-Behnken Matrix in combination with the response surface technique is preferred. In this case the "experiment" is a thermal finite element analysis, which is time consuming. Therefore, Box-Behnken Matrix sampling was used in combination with Forward-stepwise-regression. The probabilistic design loop is fully automated and, if one views this loop as a transfer function, the mean values of the three design variables can be considered as inputs ($\mu_{tgap,}$ $\mu_{R,}$ μ_{Frate}) and the mean (μ_{Tmax}, $\mu_{dT,}$ μ_{dP}) and standard deviation (σ_{Tmax}, $\sigma_{dT,}$ σ_{dP}) of the attributes (maximum temperature, differential temperature, and pressure drop) can be considered as outputs.

If a target value (upper/lower limits) or process capability indices are defined for the attributes, one may easily determine the design performance using the probabilistic loop's output variables. In our design example $T_{Target} = 55°C$, $dP_{Target} = 10$ Pa, and $dT_{Target} = 2.25°C$. T_{Target} is the maximum temperature that the battery could experience during operation; otherwise the battery life is severely compromised. dP_{Target} is selected to limit the power required for cooling and dT_{Target} is the desirable temperature difference between cells.

An alternative way to quantify the quality of the design is to determine the sigma quality level for each target by solving for "n_{maxT}, $n_{dT,}$ and n_{dP}" using the following equations.

$$\mu_{Tmax} - n_{maxT} * \sigma_{Tmax} \leq T_{Target} \quad (1)$$

$$\mu_{dT} - n_{dT} * \sigma_{dT} \leq dP_{Target} \quad (2)$$

$$\mu_{dP} - n_{dP} * \sigma_{dP} \leq dT_{Target} \quad (3)$$

The overall quality level "n" is the maximum of value of n_{maxT}, n_{dT}, and n_{dP}. Typically a six sigma quality level (n = 6) corresponds to 3.4 defects per million. If the desired sigma level of quality is achieved with the first design, the lucky designer can stop at this point. If the desired sigma level of quality is not achieved, the designer needs to adjust the controlled inputs of the probabilistic design loop ($\mu_{tgap,}$ $\mu_{R,}$ μ_{Frate}) and rerun his analysis. This adjustment can be automated with a design optimization loop.

4. The Design Optimization Loop

The two main control variables used as inputs for the probabilistic design loop are the mean value of the air gap and the flow rate. The three main outputs of that loop are the sigma quality levels of each one of the three targets. The designer's goal is to select the sets of values for the design variables ($\mu_{tgap,}$ $\mu_{R,}$ μ_{Frate}) that maximize the minimum value of the three-sigma quality levels. The optimization setup in mathematical form is:

Find the values of $\mu_{tgap,}$ $\mu_{R,}$ μ_{Frate} that				
Maximize the min [n_{maxT}, n_{dT} and n_{dP}]				
subject to the design constraints of:				
1.00 mm	<	μ_{tgap}	<	3.00 mm
0.25 scfm	<	μ_{Frate}	<	1.5 scfm

This task has been fully automated with the design optimization loop [9]. Since each "experiment" in this loop is computationally expensive, the D-optimal sampling technique was selected to choose the initial set of trials. The sequential unconstrained minimization technique was selected as the optimization method. Reference 7 shows the workflow for the optimization loop.

5. Results

5.1 Loading and Boundary Conditions

The boundary conditions applied to the thermal FEA model include convection on the top and the two flat sides of the module. The heat transfer coefficient for the top and side areas was calculated based on the airflow rate. A heat transfer coefficient of 5.0 W/m^2 K was applied at the bottom and two ends of the module. The inlet air temperature was assumed to be 25°C and varied linearly along the height of the module, with the outlet temperature calculated from:

$$T_{out} = \dot{q} / \dot{m}\ c_p + T_{in} \tag{4}$$

where c_p is heat capacity, $\dot{m}$ is mass flow rate, and $\dot{q}$ is heat generation rate inside the battery core, which also could be calculated based on internal battery resistance (R) and input current (I).

$$\dot{q} = I^2R \tag{5}$$

The input current was assumed to be constant at 15 amps. This is based on the average current levels measured during several different vehicle-driving cycles. The nominal internal resistance, based on measured values, was 0.02 ohms.

5.2 Results of the Probabilistic Analysis

A typical set of probability density functions of the parametric FEA input model are shown in Figure 4. These probability density functions represent a single point in the design space corresponding to a mean value of the air gap μ_{tgap} = 2.0 mm, standard deviation of the gap σ_{tgap} = 0.10 mm, mean value of the electric resistance of the cells μ_R = 0.01 ohms, standard deviation of the resistance σ_R = 0.001 ohms, mean value of the flow rate μ_{Frate} = 1.0 scfm, and standard deviation of the flow rate σ_{Frate} = 0.15 scfm. Executing the probabilistic design loop resulted in a probabilistic distribution of the response attributes (maxT, dT, dP).

Figure 5 shows the histogram of the maximum temperature (maxT response attribute) for the probabilistic design loop corresponding to input values shown in Figure 4. The green vertical lines are placed in standard deviation increments from the mean value. If, for example, the upper specification limit (USL) was 70°C, the quality level is $n_{maxT} = 2.6\ \sigma$, which is the distance between the target and the mean value in standard deviation units. Similarly, Figure 6 shows the histogram of the temperature differential (dT) corresponding to input values shown in Figure 4. In this case the USL is 2.25°C and the quality level is $n_{dT} = 2.15\ \sigma$. Figure 7 shows the histogram of the pressure drop (dP) corresponding to input values shown in Figure 4. In this case, USL is 10 Pa and the quality level is $n_{dP} = 3.3\ \sigma$.

All the results shown in Figures 4 -7 correspond to a single point in the design space for a given mean air gap and mean flow rate (μ_{tgap} = 2.0 mm and μ_{Frate} = 1.0 scfm). For future reference this will be design point A. The probabilistic analysis was automatically repeated for a range of values of the μ_{tgap} and μ_{Frate} and the sigma quality levels for all three requirements were found. Figure 8 shows the effect of air gap on

the quality level for the maximum temperature target (55°C) and various values of the flow rate. For maximum temperature, as the mean air gap increases the quality level decreases and as the mean flow rate increases the quality level increases. If quality was the only requirement, we could select (using Figure 8) the values of the air gap and flow rate for a desired quality level. For example, for a six-sigma quality level the mean air gap should be greater than 1.2 mm and the mean flow rate should be greater than 1.2 scfm. For future reference this will be design point B (μ_{tgap} = 1.2 mm and μ_{Frate} = 1.2 scfm).

Figure 9 shows the effect of air gap on quality level for the temperature differential target (2.5°C) and various values of flow rate. For the temperature differential, as the air gap increases the quality level decreases and as the flow rate increases the quality level increases. For the temperature differential requirement, the sigma level of design point B is about 13.

Figure 10 shows the effect of air gap on sigma quality level for the pressure drop target (2.5°C) and various values of the flow rate. For pressure drop, as the air gap increases the quality level increases and as the flow rate increases the quality level decreases (contrary to the trends observed in the previous two targets). For this design requirement, the sigma level of design point B is negative which is unacceptable. In order to obtain the best design point in the presence of conflicting requirements the sigma quality level for all three design requirements has been plotted versus the mean value of air gap in Figure 11. For air gaps less than 1.9 mm, the pressure drop target controls the design and for air gaps greater than 1.9 mm the maximum temperature target controls the design. The intersection of the maximum temperature and pressure drop curves define the best design point, as shown in Figure 11.

5.3 Transient Response

Simulating steady state analysis is very efficient mathematically, because the final air bulk temperature can be computed from a closed-form solution and the heat generation rate is constant. In order to examine the transient response of the core temperature versus time for prismatic batteries under the 40 kW FreedomCAR Power-Assist Profile [10] a transient finite element model was built and validated. Since the air bulk temperature varies versus time, a set of three-dimensional thermal fluid elements with the ability to conduct heat and transmit fluid was used. Heat flow is due to conduction within the fluid and the mass transport of the fluid. Convection from the fluid to the external battery surface is accounted for in the film coefficient that is related to the fluid flow rate.

The transient heat generation of the core is computed from the 40 kW FreedomCAR Power-Assist profile via a thermal efficiency factor. Figure 12 shows the power and heat generation for a prismatic battery module based on a battery size factor (BSF) of 38 and assuming round trip energy efficiency of 0.9. BSF represents the minimum number of modules required to meet all the FreedomCAR performance and life goals [10]. Figure 13 shows the maximum, minimum, and average core temperature versus time for the 40 kW FreedomCAR Power-Assist Profile at Palm Springs (with maximum ambient temperature 45°C per FreedomCAR test manual [10]) with high airflow rate (3 scfm). All three curves approach their corresponding steady-state values asymptotically. The high frequency variation of these curves corresponds to the frequency of the pulses within the power profile. The icon shown in Figure 13 is a partially sectioned view of the temperature distribution of the module. The left portion shows the temperature distribution of the flow channels and the outside surface of the module. The right portion shows a section view of the middle of the module (through the core). Figure 14 shows a comparison of the core temperature versus time for low (1.0 scfm) and high (3.0 scfm) airflow rates. The icons shown in Figure 14 are the temperature distributions (with the same scale) of the module at a middle plane for low and high airflow rates. The maximum differential module temperature appears at steady-state and is 4.04°C for the low flow rate and 1.75°C for the high flow rate.

From the transient thermal analysis we can observe that for a 40 kW FreedomCAR Power Profile the maximum, minimum, and average core temperatures reach their steady-state values at the same time; at

approximately 30 min. The modules with high flow rate reach their steady-state values 60% faster than the modules with low flow rate and their average temperature is 90% lower and their maximum differential module temperature is 43% lower.

6. Conclusions

This paper examined a process of using design for six-sigma to improve the robustness of battery thermal management for hybrid electric vehicles. We used finite element thermal analysis, along with optimization and design for six sigma processes to evaluate alternatives for reducing temperature distribution and improving overall temperature uniformity among cells over the range of battery operation and conditions while minimizing parasitic losses. The methods presented show how variations in input parameters and conflicting design constraints can be accounted for when designing battery thermal management systems. We applied the process to an air-cooled, prismatic NiMH module. With the existing set of design requirements imposed, only 2.5-sigma quality level achieved. Relaxing design constraints (max temperature, temperature differential, and maximum pressure drop) could result in higher-level design quality.

7. Symbols

BSF	Battery Size Factor
USL	upper specification limit
$\mathbf{c_p}$	heat capacity
$\mathbf{dP_{Target}}$	target for differential module temperature
$\mathbf{dT_{Target}}$	target for pressure drop
I	input current
$\mathbf{T_{in}}$	inlet air temperature
$\mathbf{T_{out}}$	outlet air temperature
$\mathbf{T_{target}}$	target for maximum cell temperature
μ_{tgap}	mean value of air gap between modulus
μ_R	mean value of internal cell resistance
μ_{Frate}	mean value of flow rate
μ_{Tmax}	mean value of maximum module temperature
μ_{dT}	mean value of deferential module temperature
μ_{dP}	mean value of pressure drop
$\mathbf{n_{maxT}}$	quality level for maximum temperature target
$\mathbf{n_{dT}}$	quality level for temperature differential target
$\mathbf{n_{dP}}$	quality level for pressure drop target
σ_{tgap}	standard deviation of air gap
σ_R	standard deviation of cell resistance
σ_{Frate}	standard deviation of flow rate
σ_{Tmax}	standard deviation of maximum module temperature
σ_{dT}	standard deviation of deferential module temperature
σ_{dP}	standard deviation of pressure drop
R	internal battery resistance
$\dot{\mathbf{m}}$	mass flow rate for cooling fluid
$\dot{\mathbf{q}}$	heat generation rate

8. Acknowledgments

The Department of Energy (DOE), Office of the FreedomCAR and Vehicle Technology funded this effort. The authors would like to thank Robert Kost and Tien Duong of DOE, and Ted J. Miller of Ford Motor Company, also FreedomCAR Battery Tech Team Chairman, for their support on this project.

9. Figures

Figure 1: Panasonic NiMH Battery Module (7.2V, 6.5 A) Studied

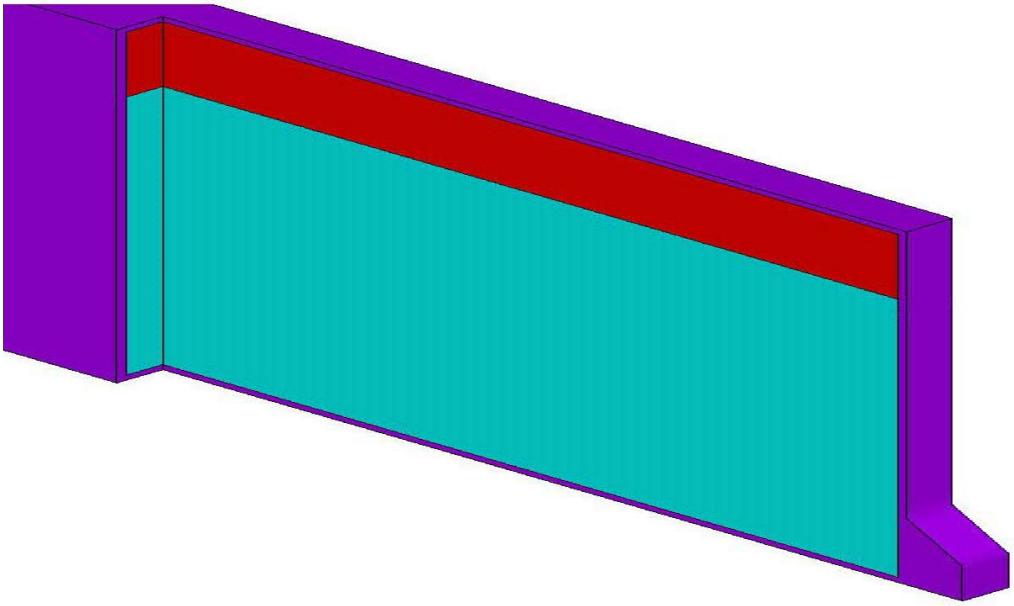

Figure 2: Parametric Solid Model of the Module in Figure 1

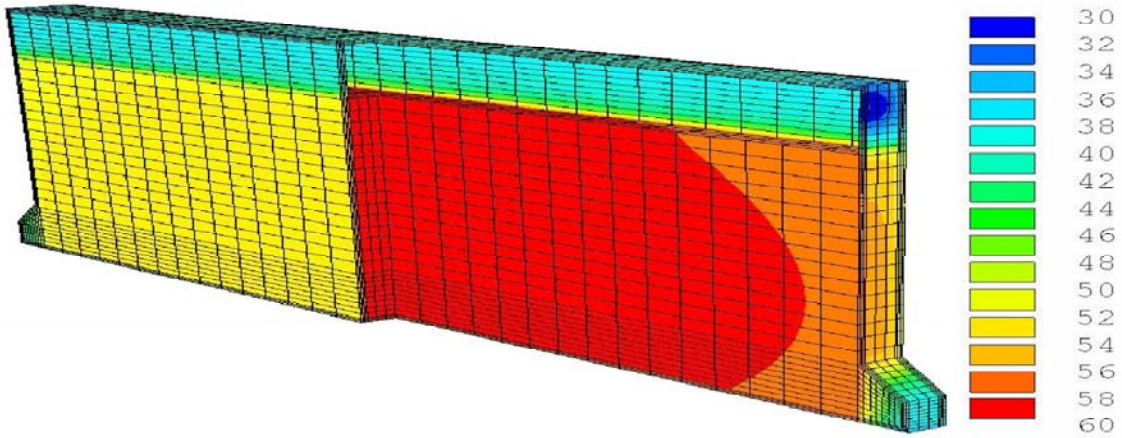

Figure 3: Typical Temperature Distribution in a Module

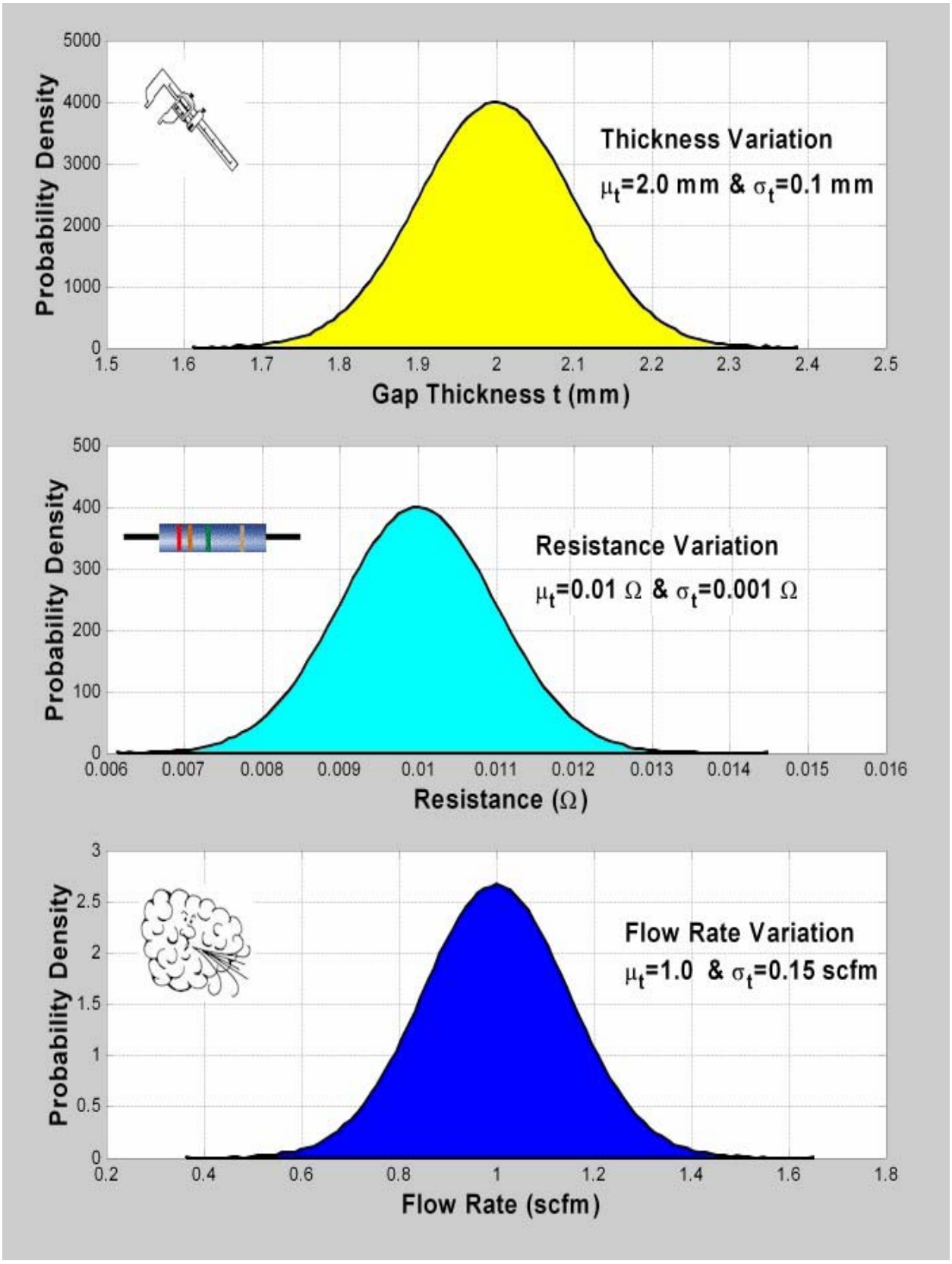

Figure 4: Probability Density Functions Of Input Parameters

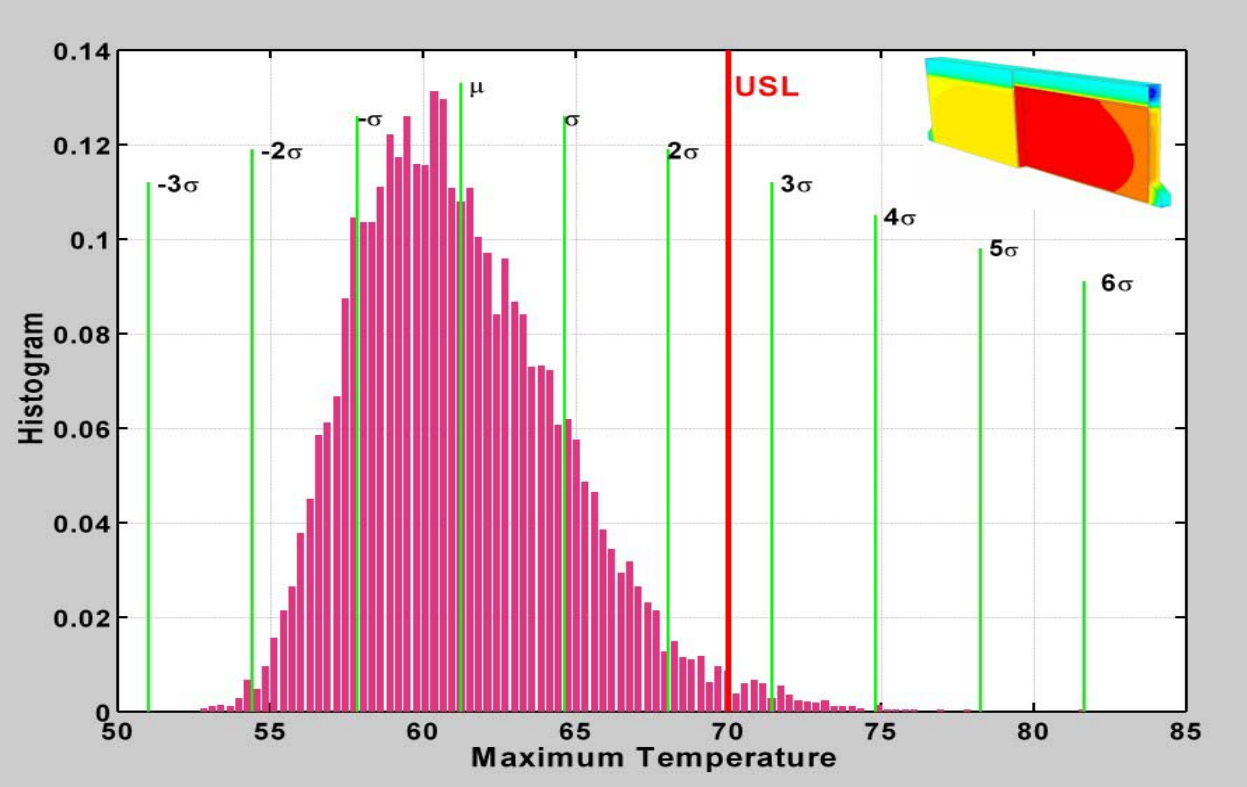

Figure 5: Histogram of maximum temperature and sigma quality levels

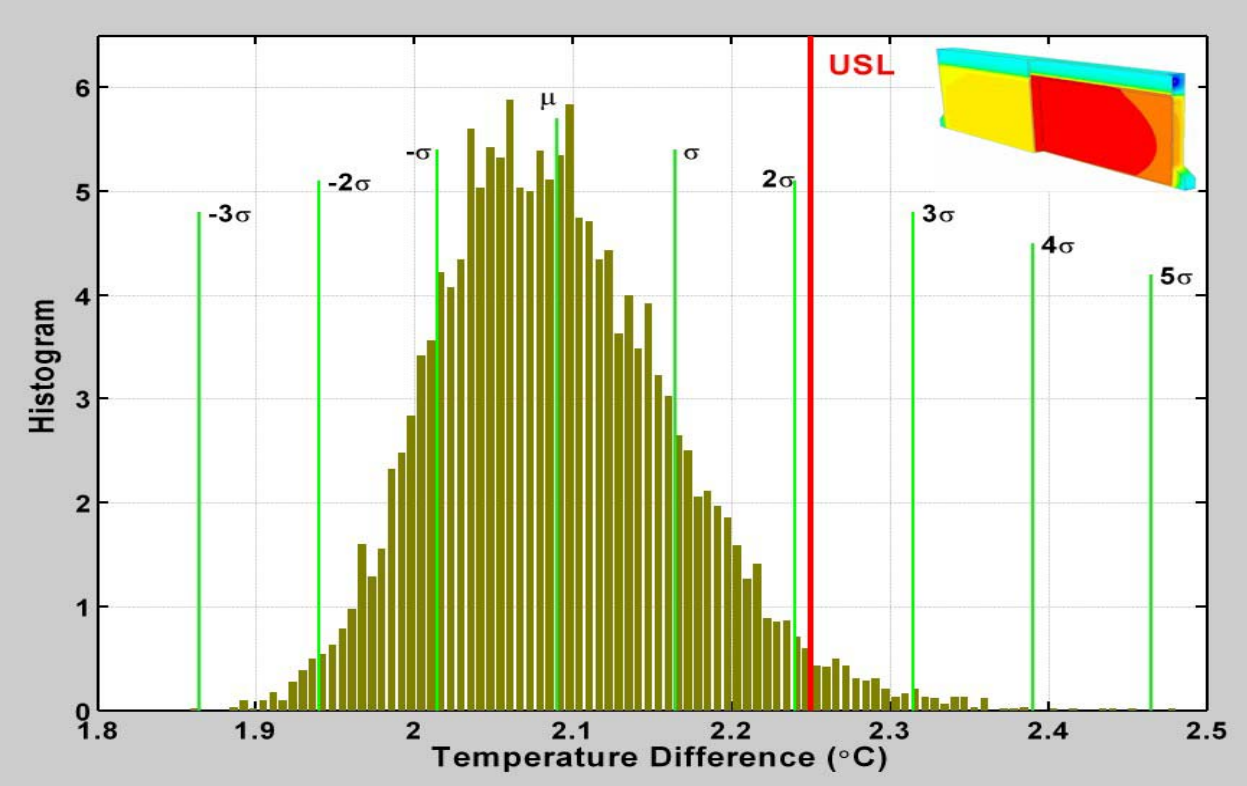

Figure 6: Histogram of temperature differential and sigma quality levels

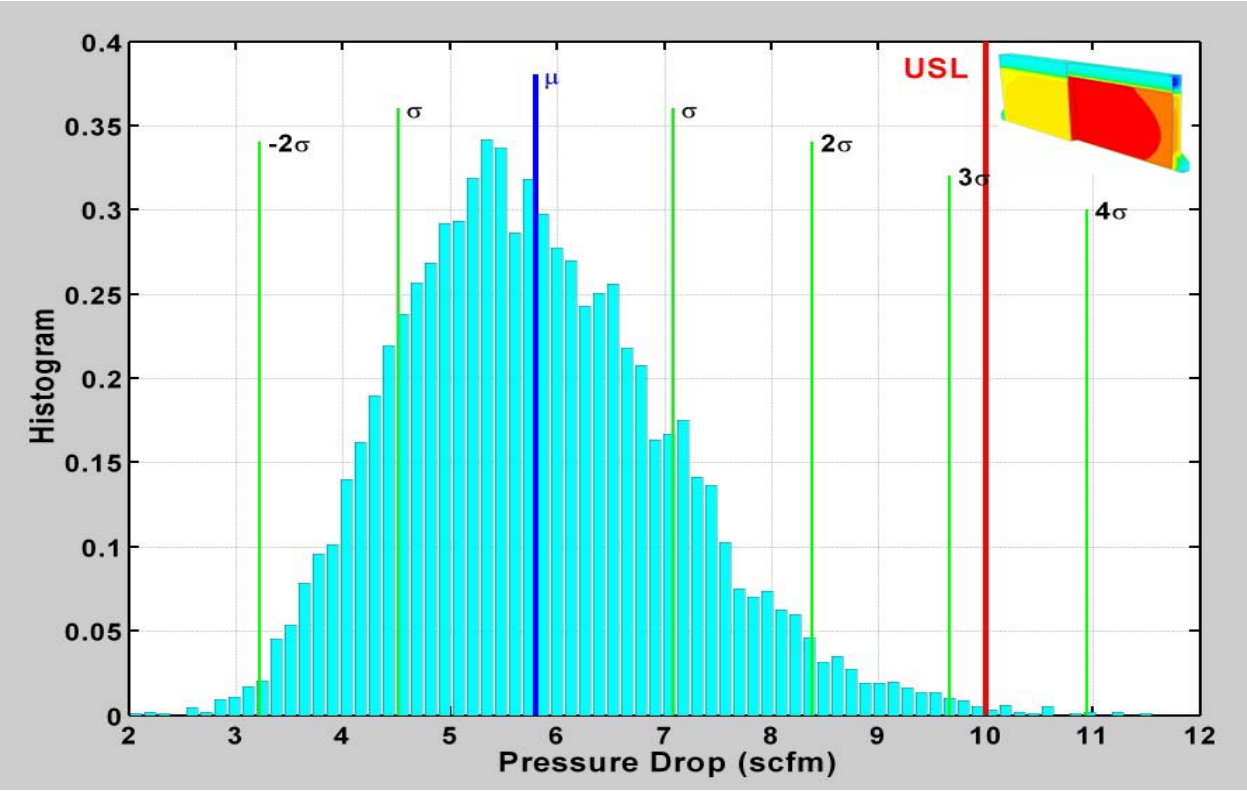

Figure 7: Histogram of pressure drop and sigma quality levels

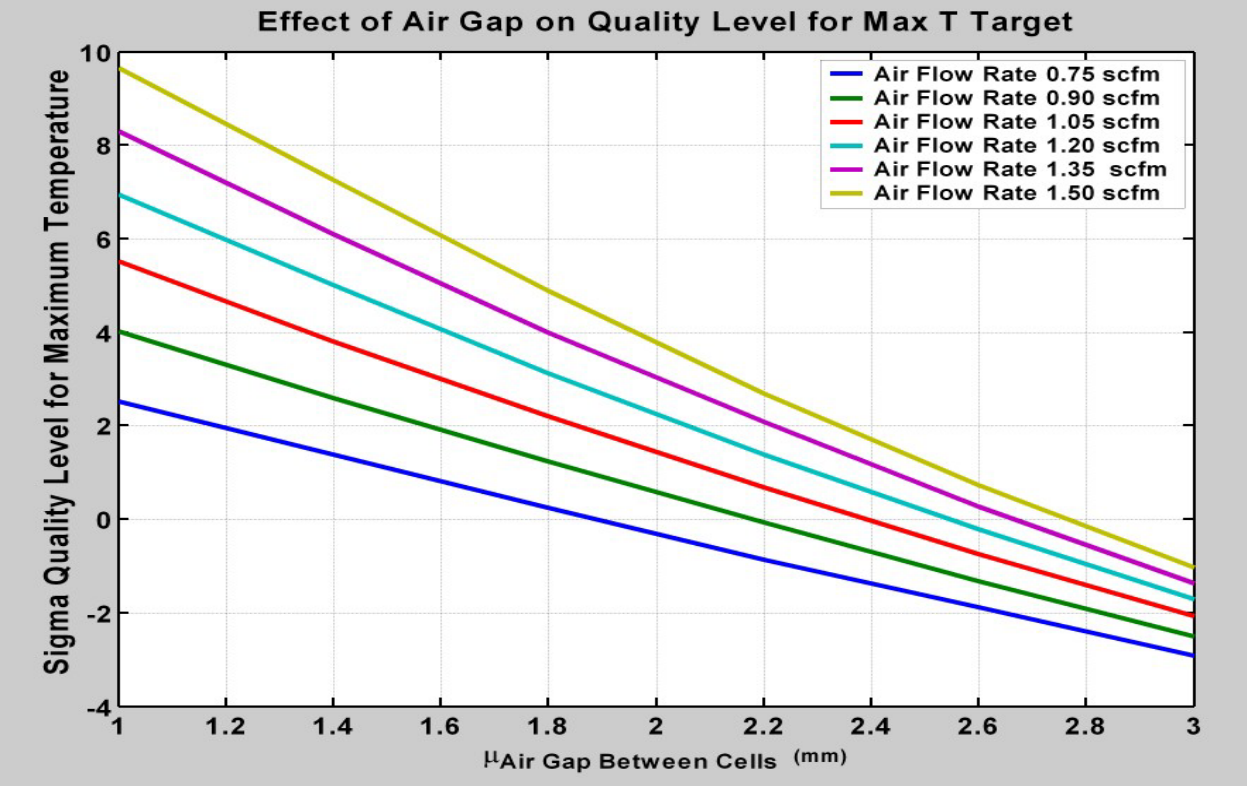

Figure 8: Effect of air gap on sigma quality level for Max Target = 55 °C

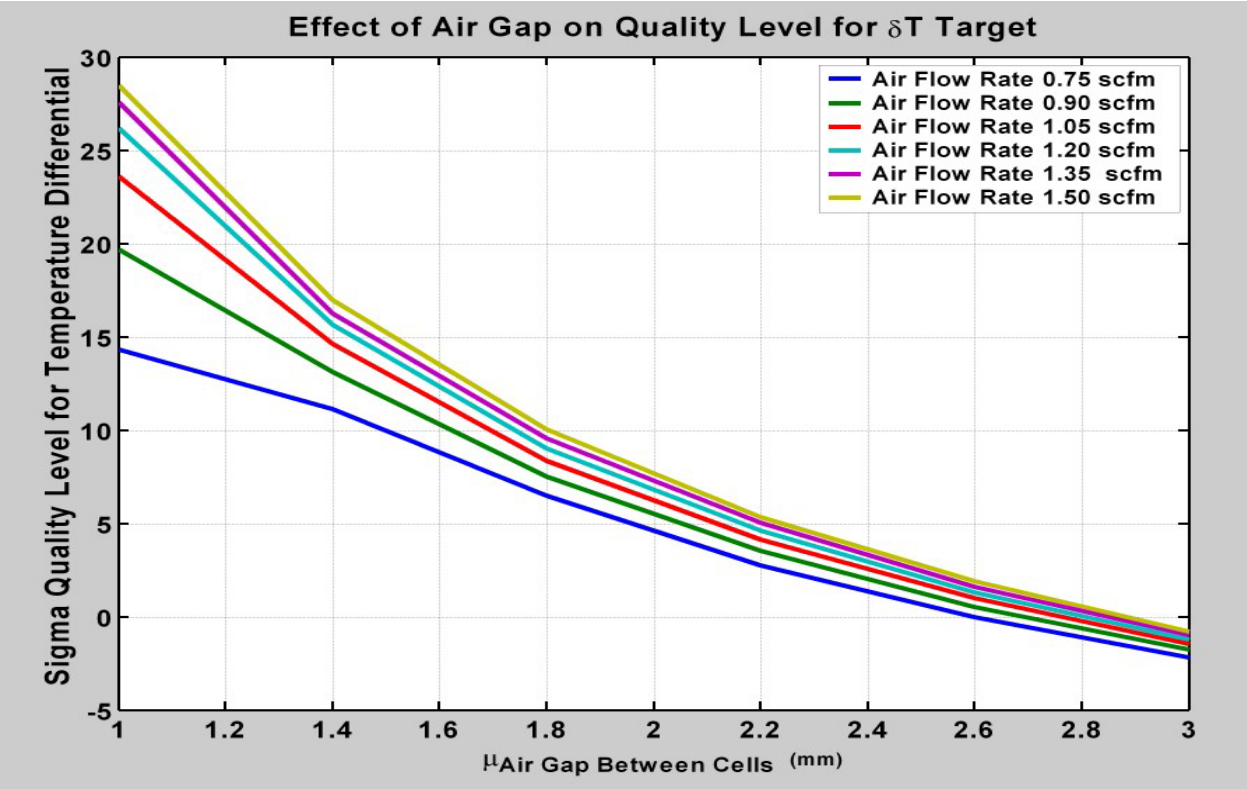

Figure 9: Effect of air gap on sigma quality level for dT Target = 2.5 °C

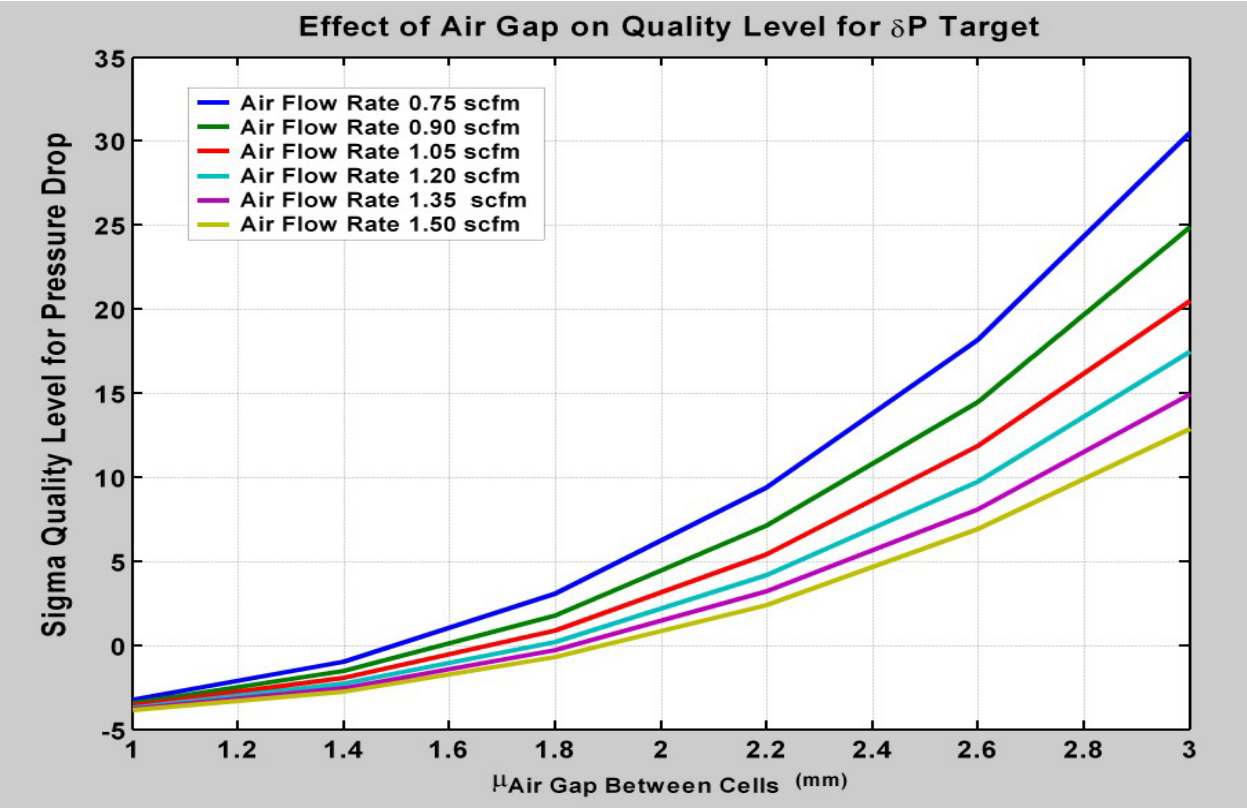

Figure 10: Effect of air gap on sigma quality level for dP Target = 10 scfm

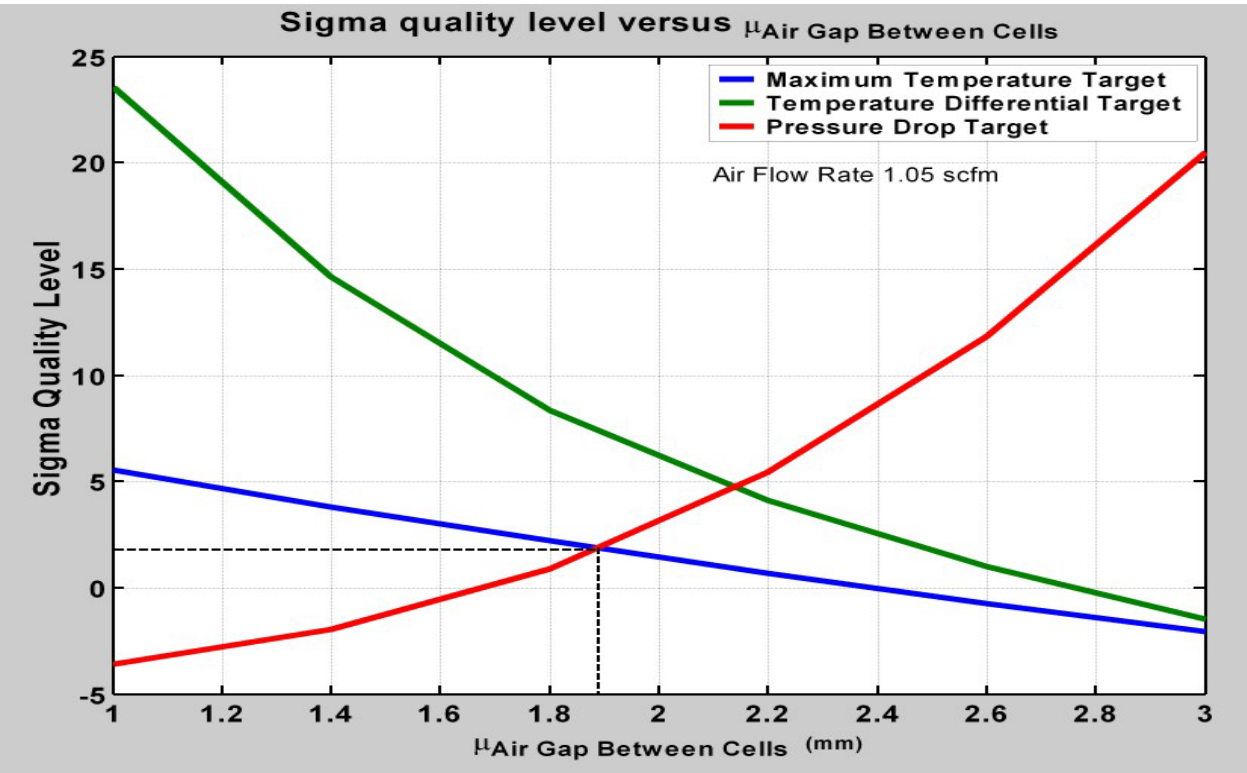

Figure 11: Effect of air gap on overall sigma quality levels

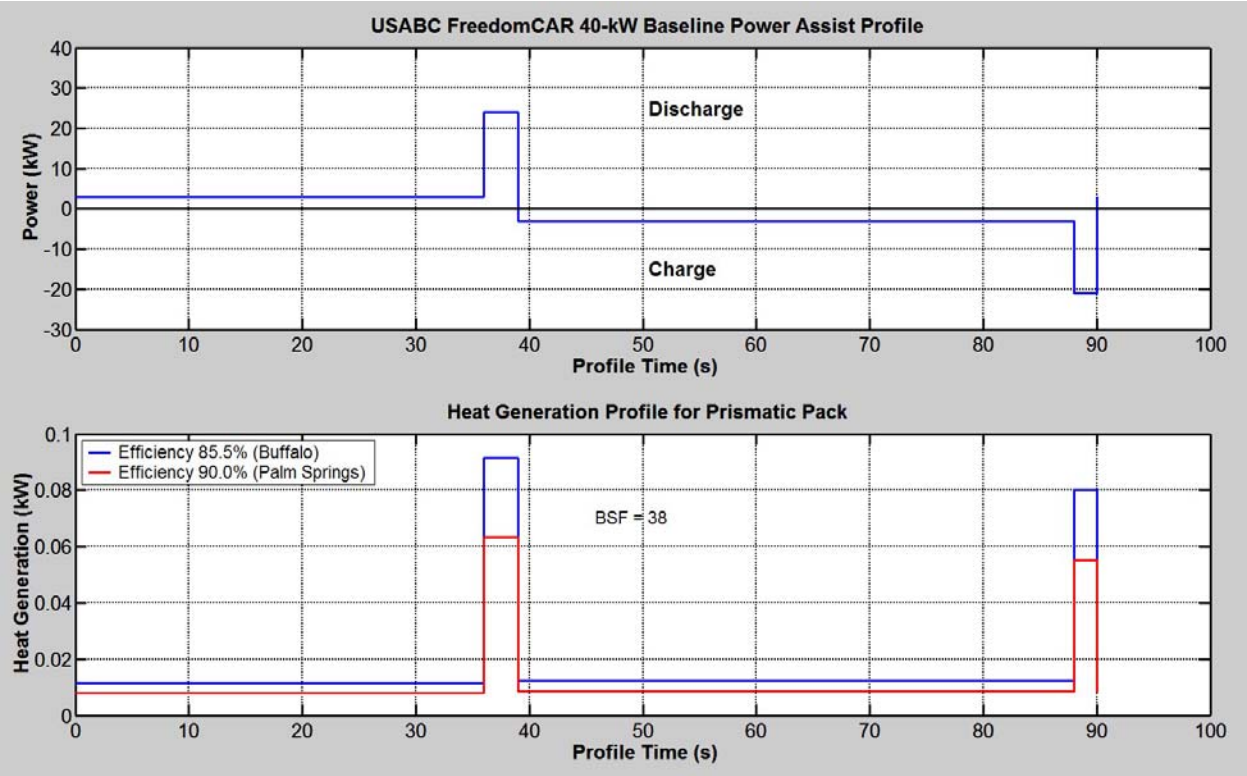

Figure 12: FreedomCAR 40-kW Baseline Power Assist and Heat Generation Profiles

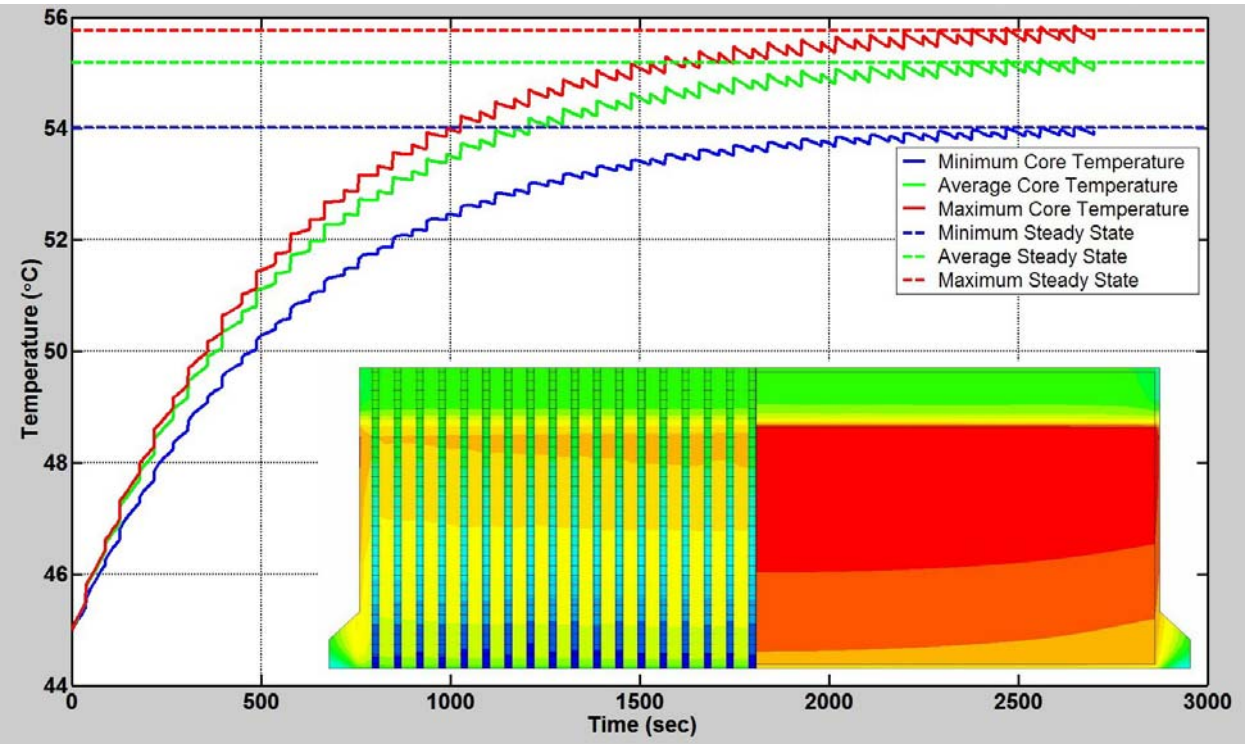

Figure 13: Core Temperature versus Time for 40 kW FreedomCAR Power Profile at Palm Springs with High Air Flow Rate

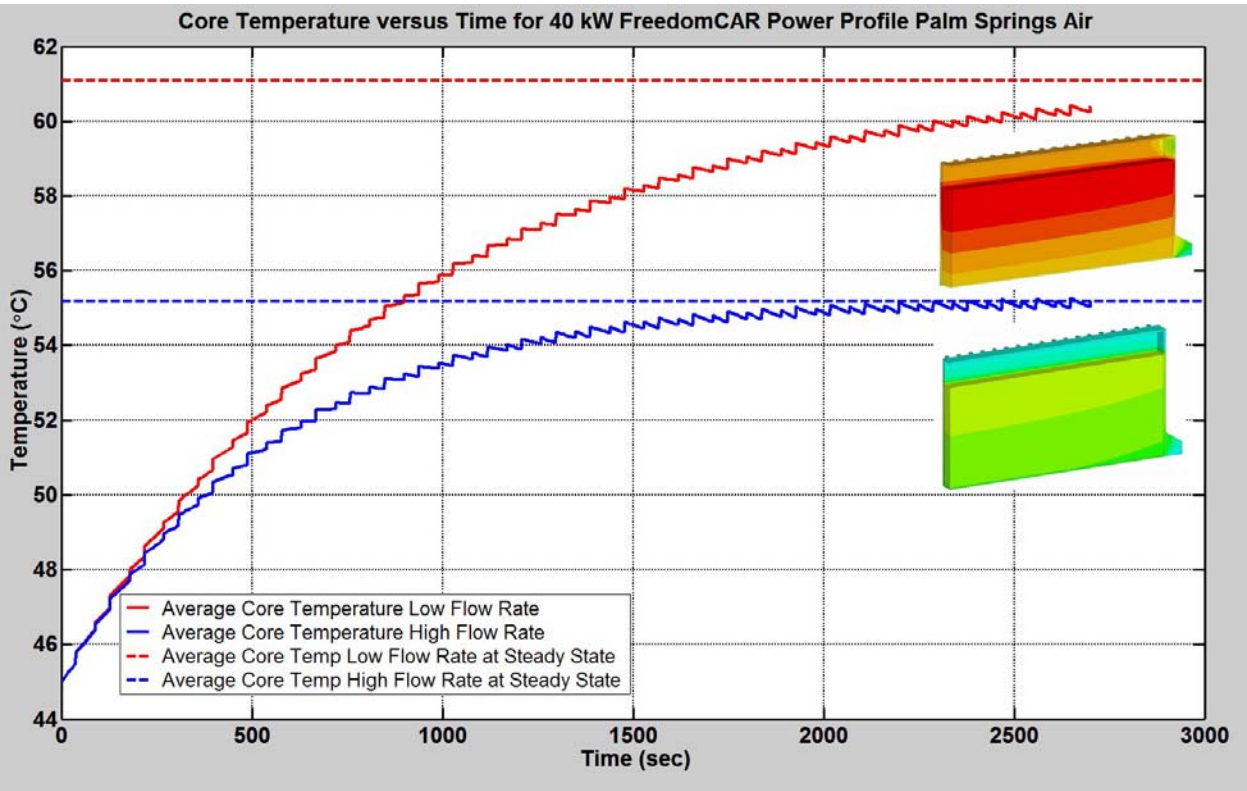

Figure 14: Average Core temperature versus time for 40 kW FreedomCAR Power Profile at Palm Springs with Low and High Air Flow Rate

10. References

[1] Zolot, M., et al, Thermal Evaluation of a Toyota Prius HEV Battery Pack (Out of Vehicle Testing), NREL/MP-540-30376, NREL, Golden, CO, May 2001.

[2] Kelly, K., Zolot, M., Mihalic, M, Battery Usage and Thermal Performance of the Toyota Prius and Honda Insight during Chassis Dynamometer Testing, 17th Annual Battery Conference on Applications and Advances, Long Beach, CA, January 2002.

[3] ANSYS Inc. Probabilistic Design Techniques, Advanced Analysis Techniques Guide, August 2002.

[4] Creveling, C., Slutsky, J., Antis, D., Design for Six Sigma : in technology & product development Prentice Hall Upper Saddle River, NJ, 2003.

[5] Breyfogle, F., Cupello, J., Meadows, B., Managing Six Sigma: a practical guide to understanding, assessing, and implementing the strategy that yields bottom-line success, John Wiley, New York 2001.

[6] Marckzyk J., Principals of Simulation-based Computer-aided Engineering, FIM Publications, September 1999.

[7] Schmidt, R. & Launsby, S., Understanding Industrial Designed Experiments, 4th ed., Air Academy Press, 2000.

[8] Vlahinos, A., Penney T. and Kelkar, S. " Engineering Quality into Digital Functional Vehicles," proceedings of IDPS2002, *2002 Daratech Intelligent Digital Prototyping Strategies Conference*, Detroit, MI, June 2002.

[9] Vlahinos A., Kelly K., Pesaran A., Penney T., "Empowering Engineers to Generate Six-Sigma Quality Designs" Proceedings of *First Annual Quality Paper Symposium, American Society for Quality, Automotive Division*, Livonia, MI, February 2003.

[10] FreedomCAR Battery Test Manual for Power-Assist HEVs, DOE/ID – 11069 draft, April 15, 2003.

11. Authors

Dr. Andreas Vlahinos is a principal of Advanced Engineering Solutions and professor adjunct at CU-Boulder. He received his Ph.D. from Georgia Institute of Technology. He has been Professor at the University of Colorado teaching courses in Structural Mechanics and Computer Aided Structural Engineering. He is several times recipient of the Professor of the Year Award. He has over 100 publications. He has been instrumental in rapid product development through the implementation of Six Sigma and Computer Aided Concurrent Engineering for Government agencies such as NREL, NASA, and DOE and industry partners in aerospace and automotive industry. He currently works with NREL extensively.

Ken Kelly is a Senior Engineer at NREL. He holds a B.S. and an M.S. in Mechanical Engineering from Ohio University. Ken has published a number of technical papers and presentations on alternative fuel vehicle (AFV) emissions. He joined NREL in 1991. In 1993, Ken took over the AFV emissions testing program. In the last few years, Ken has been working on vehicle system analysis, Computer Aided Design tools, Digital Functional Vehicles, heavy hybrids, and design using Six Sigma quality.

John Rugh is a Senior Engineer at NREL. He holds a B.S. from Colorado State University and an M.S. in Heat Transfer and Thermodynamics from Purdue University. At Purdue, John designed and built a test apparatus to determine the ideal and actual performance of an automobile heat exchanger. After working in Lockheed Martin, John joined NREL in 1998 as a member of the hybrid vehicle team. Currently he is working on the ancillary load reduction project and thermal management of advanced vehicles. Specific tasks include vehicle thermal testing, passenger compartment thermal/fluid modeling, and prediction of human thermal comfort.

Ahmad Pesaran is a Principal Engineer at the NREL and is the Project Manager for energy storage and thermal management activities. He received his Ph.D. from UCLA. Ahmad joined NREL in 1983 and has worked on various energy systems including solar cooling, air conditioning, desiccant dehumidification/cooling, and most recently hybrid electric vehicles. He has been working on hybrid electric vehicle projects since 1995 where he has established facilities and analytical capabilities in thermal analysis and management of energy storage devices.